arXiv:0912.0199v4 [hep-ph] 26 Mar 2010

Next-to-leading order QCD predictions for graviton and photon associated production in the Large Extra Dimensions model at the LHC

Xiangdong Gao, Chong Sheng Li,* Jun Gao, and Jian Wang

Department of Physics and State Key Laboratory of Nuclear Physics and Technology, Peking University, Beijing 100871, China

Robert J. Oakes

Department of Physics and Astronomy, Northwestern University, Evanston, Illinois, 60208-3112, USA

(Dated: March 29, 2010)

Abstract

We present the calculations of the complete next-to-leading order(NLO) QCD corrections to the inclusive total cross sections for the Kaluza-Klein(KK) graviton and photon associated production process $pp \to \gamma G_{KK} + X$ in the large extra dimensions model at the LHC. We show that the NLO QCD corrections in general enhance the total cross sections and reduce the dependence of the total cross sections on the factorization and renormalization scales. When jet veto is considered, the NLO corrections reduce the total cross sections. We also calculate some important differential cross sections for this process at NLO: the missing transverse momentum distribution, the transverse momentum distribution and the pseudorapidity distribution of photon.

PACS numbers: 11.10.Kk, 12.38.Bx, 13.85.Qk, 14.80.Rt

*Electronic address: csli@pku.edu.cn

I. INTRODUCTION

The idea that the extra dimensions theory can appear at the TeV scale, well below the Planck scale $M_P \sim 1.2 \times 10^{19}$GeV, was proposed in the 1990s[1–10] and promises rich phenomenology at the TeV scale. Now the search for extra dimensions is one of the important tasks for the LHC.

Among various extra dimensions models the large extra dimensions(LED) model introduced in Ref.[1–3] is the first TeV scale gravity theory and has been extensively studied[11, 12]. In this model space-time has $4+\delta$ dimensions and the standard model(SM) particles reside in the usual $3+1$-dimensional SM brane and can not propagate in the extra δ-dimensional space, which is assumed to be compacted on a torus with a common radius R, while gravity can propagate in the whole $4+\delta$ dimensional world. From the view of our 4-dimensional world, there exists infinitely many Kaluza-Klein(KK) modes of gravitons with mass $|k|/R$ interacting with SM particles, where $k^2 = \sum_{i=1}^{\delta} k_i^2$ with k_i being the integer. The 4-dimensional Planck scale is no longer the fundamental scale, but an effective scale in the 4-dimensional world, and is related to a fundamental scale M_D ∼TeV by the Newtonian law of gravitation in $4+\delta$ dimensions[1, 12]

$$\bar{M}_P \equiv M_P/\sqrt{8\pi} = R^{\delta/2} M_D^{1+\delta/2}, \tag{1}$$

where $\bar{M}_P$ is the reduced Planck mass. According to Eq.(1), deviations from the usual Newtonian gravitational law appear at $R \sim 10^{\frac{32}{\delta}-19}$ meters, which is not a conflict with the current gravitational experiments[13] once $\delta \geq 2$. Before further results of terrestrial gravitational experiments appear, one may resort to colliders to find signals of this model. Although, in this model the couplings of gravitons to SM particles are suppressed by $1/M_P$ [11, 12], the summation of the production of large numbers of KK modes with arbitrary mass smaller than M_D may compensate for this suppression and lead to observable effects. There are two ways to probe such effects at colliders: graviton emission and virtual graviton exchange, which have been investigated in Ref. [11, 12, 14]. As shown in Ref.[12], because of the suppression of the couplings of gravitons to SM particles, the decays of gravitons to SM particles have a small probability to occur before they propagate into the extra δ-dimensional space, which means the gravitons behave like massive, stable, and noninteracting particles once they are produced. Thus, the signal for graviton and photon associated production at the LHC is a single photon plus missing energy. Since the electromagnetic coupling is small

and the $q\bar{q}$ luminosity is lower than for gg at the LHC the rate for this process is much smaller than for jet and graviton associated production. But the photon signal would be a clean signature; and in case of discovery in jet plus graviton events, the photon plus graviton signal would provide a useful independent test[12]. Only leading-order(LO) calculations and analysis of the process were performed in Ref.[12]. Since LO cross sections for processes at hadron colliders suffer from large uncertainties due to the choices of the renormalization scale (μ_r) and factorization scale (μ_f) and higher order QCD corrections are generally large and can improve the scale uncertainties at hadron colliders. Several works[15–23] have performed next-to-leading order(NLO) QCD corrections in extra dimensions models. In this paper we present the complete calculations of NLO QCD corrections to this process which improve the theoretical predictions.

This paper is organized as follows. In Sec.II we show the analytic results of the LO calculations and define the notation. In Sec.III we present the details of the calculations of both the virtual and real parts of the NLO QCD corrections. In Sec.IV we give the numerical predictions for inclusive and differential cross sections at the LHC. We close this paper with a brief conclusion. For completeness, the relevant Feynman rules are collected in Appendix A and the lengthy analytic expressions of the results of our calculations are summarized in Appendix B.

II. LEADING-ORDER CALCULATIONS

The KK gravitons with different masses can be produced at colliders only if kinematically allowed. Contributions from the different KK modes then must be summed up. Since the KK graviton mass separation of $\mathcal{O}(1/R)$ is much smaller than all the other physical scales involved, we can replace the discrete summation of different KK modes by a continuous integration. In general, the differential cross section for graviton production can be expressed as[12]

$$\frac{d^2\sigma}{dt\ dm} = S_{\delta-1}\frac{\bar{M}_P^2}{M_D^{2+\delta}}m^{\delta-1}\frac{d\sigma_m}{dt} \tag{2}$$

with

$$S_{\delta-1} = \frac{2\pi^{\delta/2}}{\Gamma(\delta/2)}, \tag{3}$$

where $S_{\delta-1}$ is the surface of a unit-radius sphere in δ dimensions and $d\sigma_m/dt$ is the differential cross section for producing a single KK graviton of mass m. Throughout this work we

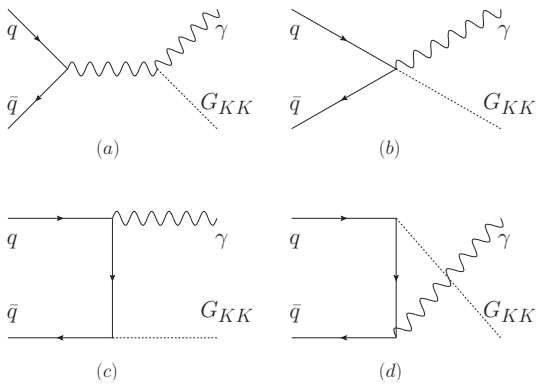

FIG. 1: Leading-order Feynman diagrams for $q\bar{q} \to \gamma G_{KK}$.

perform the integration on m from $0.1M_D$ to M_D.

The leading-order Feynman diagrams for the graviton and photon associated production process $q(p_1)\bar{q}(p_2) \to \gamma(p_3)G_{KK}(p_4)$ are shown in Fig. 1. The related Feynman rules are given in Ref. [11, 12] and are collected in Appendix A. The LO amplitudes have been given in Ref.[11] so we need only to show the amplitudes squared here. In the LED model the spin sum over the polarization tensors of the graviton is

$$\sum_{s=1}^{5} \epsilon^{s}_{\mu\nu}\epsilon^{s*}_{\alpha\beta} = P_{\mu\nu\alpha\beta}, \tag{4}$$

with

$$P_{\mu\nu\alpha\beta} = \eta_{\mu\alpha}\eta_{\nu\beta} + \eta_{\mu\beta}\eta_{\mu\alpha} - \frac{2}{n-1}\eta_{\mu\nu}\eta_{\alpha\beta} + ..., \tag{5}$$

where the dots represent terms proportional to the graviton momentum p_4^μ and $p_4^\mu T_{\mu\nu} = 0$, giving no contribution to the amplitude. We performed our calculations in $n = 4 - 2\epsilon$ dimensions.

The LO partonic cross section is then

$$\hat{\sigma}^B_m = \frac{1}{2s}\int d\Gamma_2 \overline{\sum}|M^B|^2, \tag{6}$$

with

$$\begin{aligned}\overline{\sum}|M^B|^2 \;=\; & \frac{\mathrm{eQ}^2\kappa^2}{24stu}\left[(s+4t)m^6 - 6t(s+2t)m^4 + \left(s^3+6ts^2+18t^2s+16t^3\right)m^2\right. \\ & \left. -4t\left(s^3+3ts^2+4t^2s+2t^3\right)\right],\end{aligned} \tag{7}$$

where $\kappa = \sqrt{2}/\bar{M}_P$, s, t, and u are the Mandelstam variables defined as

$$s = (p_1+p_2)^2, \quad t = (p_1-p_3)^2, \quad u = (p_1-p_4)^2, \tag{8}$$

and $\overline{\sum}$ means that the colors and spins of the outgoing particles have been summed over and the colors and spins of the incoming particles have been averaged over. Equation(7) is a coincidence with the result shown in Ref.[12].

The LO total cross section can be obtained by convoluting the partonic cross sections with the parton distribution functions(PDF) $G_{q,\bar{q}}$ in the protons:

$$\sigma_m^B = \int dx_1 dx_2 [G_{q/p}(x_1,\mu_f) G_{\bar{q}/p}(x_2,\mu_f) + G_{q/p}(x_2,\mu_f) G_{\bar{q}/p}(x_1,\mu_f)] \hat{\sigma}_m^B. \tag{9}$$

Here μ_f is the factorization scale.

III. NEXT-TO-LEADING ORDER CALCULATIONS

The NLO corrections to the associated production of a graviton and a photon can be separated into the virtual corrections arising from loop diagrams of colored particles and the real corrections arising from the radiation of a real gluon or a massless (anti)quark. We carried out the calculations in the 't Hooft-Feynman gauge and used dimensional regularization[24] in $n = 4 - 2\epsilon$ dimensions to regulate all the ultraviolet(UV), soft and collinear divergences. We performed two independent calculations for both the analytical and numerical results for cross checking, and the results of the two groups agree with each other.

A. Virtual corrections

The Feynman diagrams for the virtual corrections to $q\bar{q} \to \gamma G_{KK}$ are shown in Fig.2 and Fig.3. They consist of self-energy, vertex, triangle and box diagrams. In order to remove the UV divergence we adopt the on-shell renormalization scheme[25–28].

We denote the bare and renormalized quark wave functions by ψ_{q0} and ψ_q, respectively. The renormalization constant δZ_q is then defined by

$$\psi_{q0} = (1 + \delta Z_q)^{1/2} \psi_q. \tag{10}$$

Calculating the quark self-energy diagram we obtain the explicit expression for δZ_q:

$$\delta Z_q = \frac{\alpha_s}{4\pi} C_F (\frac{1}{\epsilon} - \frac{1}{\epsilon_{UV}}). \tag{11}$$

Here $C_F = \frac{4}{3}$ while $1/\epsilon$ and $1/\epsilon_{UV}$ represent infrared(IR) and UV divergences, respectively.

After renormalization the UV divergences in the virtual corrections are removed leaving the IR divergences and the finite terms. The $\mathcal{O}(\alpha_s)$ virtual corrections to the partonic total cross section can then be expressed as

$$\hat{\sigma}_m^V = \frac{1}{2s}\int d\Gamma_2 \overline{\sum}\left[\frac{\alpha_s}{2\pi}\frac{\Gamma(1-\epsilon)}{\Gamma(1-2\epsilon)}\left(\frac{4\pi\mu_r^2}{s}\right)^{\epsilon}\left(\frac{2A_2^V}{\epsilon^2}+\frac{2A_1^V}{\epsilon}\right)|M^B|^2+\frac{\alpha_s}{2\pi}\mathcal{S}\right], \tag{12}$$

with

$$A_2^V = -C_F, \quad A_1^V = -\frac{3}{2}C_F. \tag{13}$$

Here $\mathcal{S}$ represents finite terms in the virtual corrections and the explicit expressions are given in Appendix B. The cancellation of IR divergent terms $1/\epsilon^2$ and $1/\epsilon$ will be discussed in detail below.

B. Real gluon emission

The Feynman diagrams for the real gluon emission process $q(p_1)\bar{q}(p_2) \to \gamma(p_3)G_{KK}(p_4) + g(p_5)$ are shown in Fig. 4.

The phase space integration for the real gluon emission will produce soft and collinear singularities which can be conventionally isolated by slicing the phase space into different regions using suitable cutoffs. In this paper we use the two-cutoff phase space slicing method[29], which introduces two arbitrary small cutoffs; i.e., a soft cutoff δ_s and a collinear cutoff δ_c, to divide the three-body phase space into three regions.

First, the phase space is separated into two regions by the soft cutoff δ_s, according to whether the energy of the emitted gluon is soft; i.e., $E_5 \leq \delta_s\sqrt{s}/2$, or hard; i.e., $E_5 > \delta_s\sqrt{s}/2$. Then the parton level real cross section $\hat{\sigma}_m^R$ can be written as

$$\hat{\sigma}_m^R = \hat{\sigma}_m^S + \hat{\sigma}_m^H, \tag{14}$$

where $\hat{\sigma}_m^S$ and $\hat{\sigma}_m^H$ are the contributions from the soft and hard regions, respectively. $\hat{\sigma}_m^S$ contains all the soft divergences, which can explicitly be obtained after the integration over the phase space of the emitted gluon. Next, in order to isolate the remaining collinear divergences from $\hat{\sigma}_m^H$, the collinear cutoff δ_c is introduced to further split the hard gluon phase space into two regions, according to whether the Mandelstam variables $t_{i5} \equiv (p_i - p_5)^2$, with $i = 1, 2$, satisfy the collinear condition $-\delta_c s < t_{i5} < 0$ or not. We then have

$$\hat{\sigma}_m^H = \hat{\sigma}_m^{HC} + \hat{\sigma}_m^{\overline{HC}}, \tag{15}$$

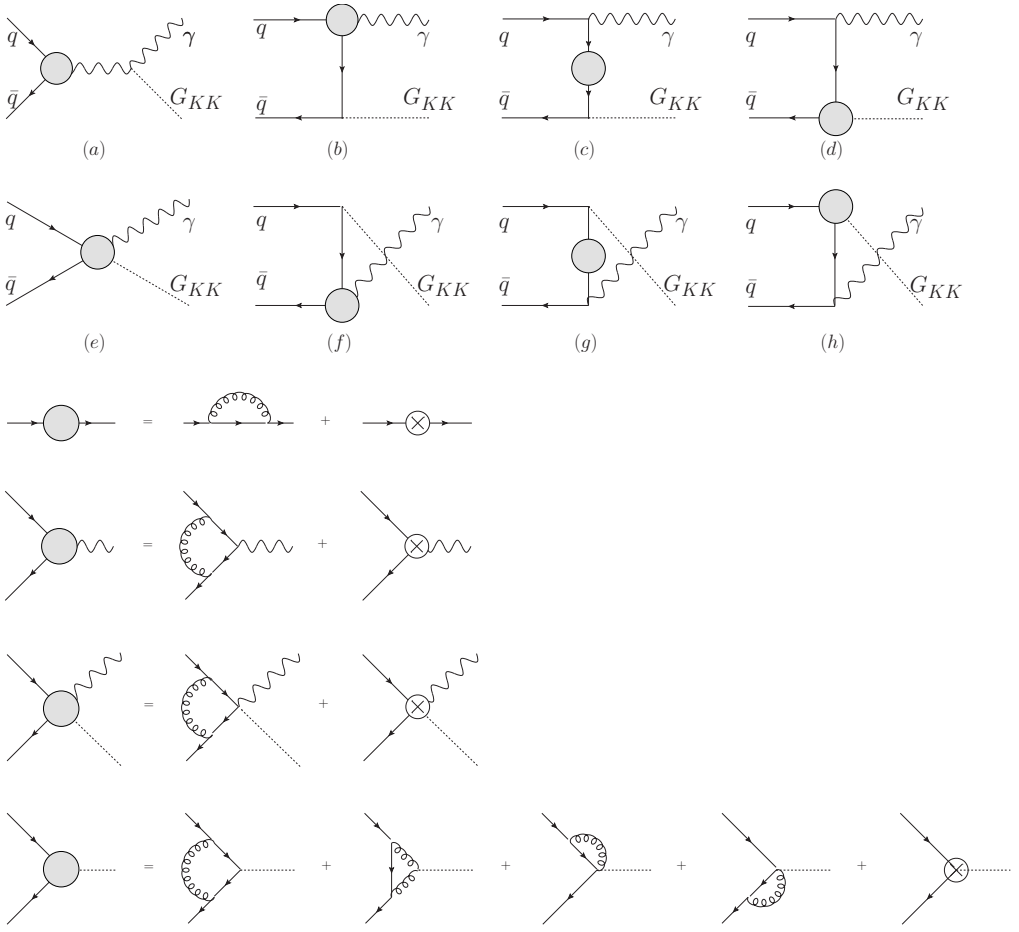

FIG. 2: One-loop virtual diagrams including vertex and self-energy corrections to $q\bar{q} \to \gamma G_{KK}$. Each brown vertex is UV divergence free.

where the hard collinear part $\hat{\sigma}_m^{HC}$ contains the collinear divergences, which also can explicitly be obtained after the integration over the phase space of the emitted gluon. The hard noncollinear part $\hat{\sigma}_m^{\overline{HC}}$ is finite and can be numerically computed using standard Monte Carlo integration techniques[30] and can be written in the form

$$d\hat{\sigma}_m^{\overline{HC}} = \frac{1}{2s}\overline{\sum}|M^{q\bar{q}}|^2 d\overline{\Gamma}_3. \tag{16}$$

Here $d\overline{\Gamma}_3$ is the hard noncollinear region of the three-body phase space.

In the next two subsections we will discuss in greater detail the soft and hard collinear

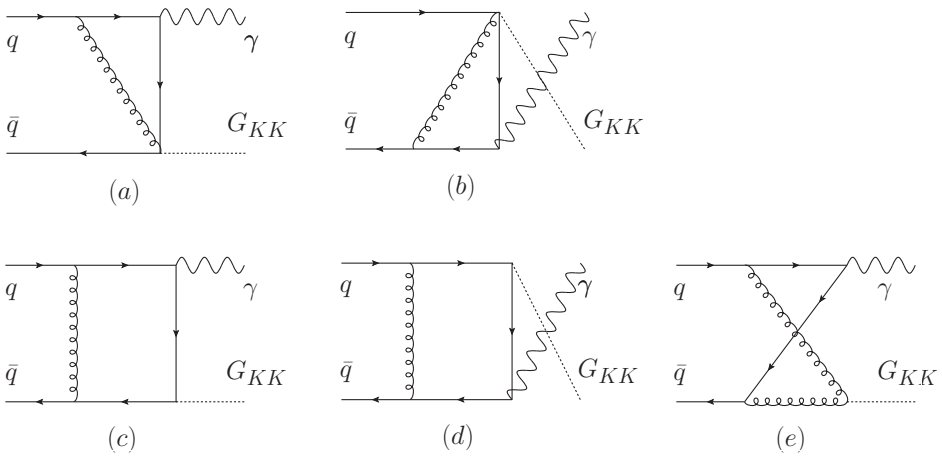

FIG. 3: Box and triangle diagrams for $q\bar{q} \to \gamma G_{KK}$. The UV divergences cancel among the five diagrams.

gluon emission.

1. Soft gluon emission

In the limit that the energy of the emitted gluon becomes small, i.e. $E_5 \leq \delta_s \sqrt{s}/2$, the amplitude squared $\overline{\sum}|M(q\bar{q} \to \gamma G_{KK} + g)|^2$ can be factorized into the Born amplitude squared times an eikonal factor $\Phi_{\rm eik}$:

$$\overline{\sum}|M(q\bar{q} \to \gamma G_{KK} + g)|^2 \xrightarrow{\rm soft} (4\pi\alpha_s\mu_r^{2\epsilon})\overline{\sum}|M^B|^2\Phi_{\rm eik}, \tag{17}$$

where the eikonal factor is given by

$$\Phi_{\rm eik} = C_F \frac{s}{(p_1 \cdot p_5)(p_2 \cdot p_5)}. \tag{18}$$

Moreover, the three-body phase space in the soft limit can also be factorized:

$$d\Gamma_3(q\bar{q} \to \gamma G_{KK} + g) \xrightarrow{\rm soft} d\Gamma_2(q\bar{q} \to \gamma G_{KK}) dS. \tag{19}$$

Here dS is the integration over the phase space of the soft gluon and is given by[29]

$$dS = \frac{1}{2(2\pi)^{3-2\epsilon}} \int_0^{\delta_s\sqrt{s}/2} dE_5 E_5^{1-2\epsilon} d\Omega_{2-2\epsilon}. \tag{20}$$

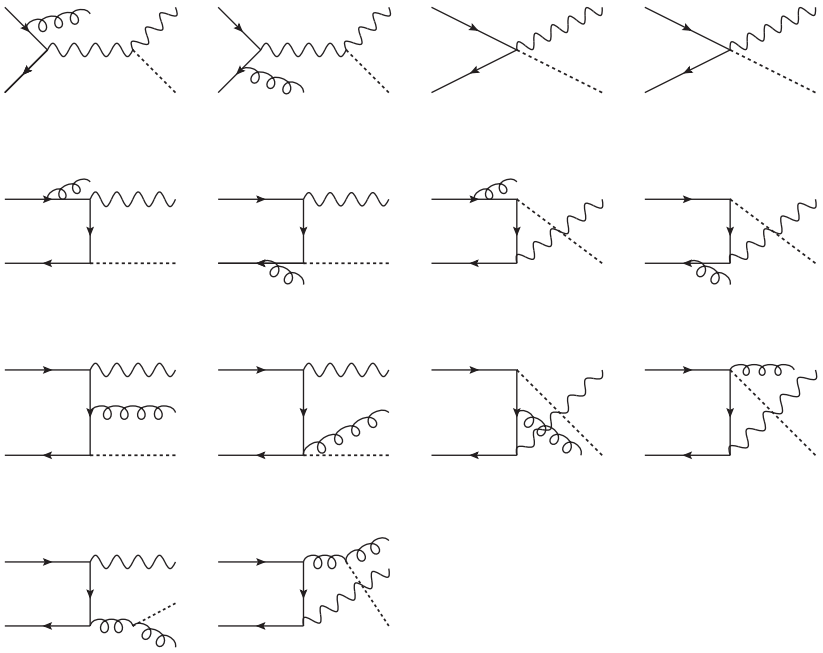

FIG. 4: Feynman diagrams for $q\bar{q} \to \gamma G_{KK} + g$.

The parton level cross section in the soft region can then be expressed as

$$\hat{\sigma}_m^S = (4\pi\alpha_s\mu_r^{2\epsilon}) \int d\Gamma_2 \overline{\sum} |M^B|^2 \int dS\Phi_{\rm eik}. \tag{21}$$

Using the approach in Ref.[29], after integration over the soft gluon phase space, Eq.(21) becomes

$$\hat{\sigma}_m^S = \hat{\sigma}_m^B \left[\frac{\alpha_s}{2\pi}\frac{\Gamma(1-\epsilon)}{\Gamma(1-2\epsilon)}\left(\frac{4\pi\mu_r^2}{s}\right)^{\epsilon}\right]\left(\frac{A_2^s}{\epsilon^2} + \frac{A_1^s}{\epsilon} + A_0^s\right) \tag{22}$$

with

$$A_2^s = 2C_F, \quad A_1^s = -4C_F \log\delta_s, \quad A_0^s = 4C_F \log^2\delta_s. \tag{23}$$

2. Hard collinear gluon emission

In the hard collinear region, $E_5 > \delta_s\sqrt{s}/2$ and $-\delta_c s < t_{i5} < 0$, the emitted hard gluon is collinear to one of the incoming partons. As a consequence of the factorization theorem[31, 32] the matrix element squared for $q\bar{q} \to \gamma G_{KK} + g$ can be factorized into the product of the Born amplitude squared and the Altarelli-Parisi splitting function for $q(\bar{q}) \to q(\bar{q})g$[33–37];

that is,

$$\overline{\sum}|M(q\bar{q}\to\gamma G_{KK}+g)|^2 \overset{\text{collinear}}{\longrightarrow} (4\pi\alpha_s\mu_r^{2\epsilon})\overline{\sum}|M^B|^2\left(\frac{-2P_{qq}(z,\epsilon)}{zt_{15}}+\frac{-2P_{\bar{q}\bar{q}}(z,\epsilon)}{zt_{25}}\right), \quad (24)$$

where z denotes the fraction of the momentum of the incoming parton carried by $q(\bar{q})$ with the emitted gluon taking a fraction $(1-z)$. $P_{ij}(z,\epsilon)$ are the unregulated splitting functions in $n=4-2\epsilon$ dimensions for $0<z<1$ which can be related to the usual Altarelli-Parisi splitting kernels[33] as follows: $P_{ij}(z,\epsilon)=P_{ij}(z)+\epsilon P'_{ij}(z)$. Explicitly

$$P_{qq}(z)=P_{\bar{q}\bar{q}}(z)=C_F\frac{1+z^2}{1-z}+C_F\frac{3}{2}\delta(1-z), \quad (25)$$

$$P'_{qq}(z)=P'_{\bar{q}\bar{q}}(z)=-C_F(1-z)+C_F\frac{1}{2}\delta(1-z). \quad (26)$$

Moreover, the three-body phase space can also be factorized in the collinear limit and, for example, in the limit $-\delta_c s<t_{15}<0$ it has the following form[29]:

$$d\Gamma_3(q\bar{q}\to\gamma G_{KK}+g)\overset{\text{collinear}}{\longrightarrow} d\Gamma_2(q(\bar{q})\to\gamma G_{KK};s'=zs)\frac{(4\pi)^\epsilon}{16\pi^2\Gamma(1-\epsilon)}dzdt_{15}[-(1-z)t_{15}]^{-\epsilon}. \quad (27)$$

Here the two-body phase space should be evaluated at a squared parton-parton energy of zs. Thus the three-body cross section in the hard collinear region is given by[29]

$$\begin{aligned} d\sigma_m^{HC} \;=\; & d\hat{\sigma}_m^B\left[\frac{\alpha_s}{2\pi}\frac{\Gamma(1-\epsilon)}{\Gamma(1-2\epsilon)}\left(\frac{4\pi\mu_r^2}{s}\right)^\epsilon\right](-\frac{1}{\epsilon})\delta_c^{-\epsilon}\left[P_{qq}(z,\epsilon)G_{q/p}(x_1/z)G_{\bar{q}/p}(x_2)\right. \\ & \left.+P_{\bar{q}\bar{q}}(z,\epsilon)G_{\bar{q}/p}(x_1/z)G_{q/p}(x_2)+(x_1\leftrightarrow x_2)\right]\frac{dz}{z}\left(\frac{1-z}{z}\right)^{-\epsilon}dx_1dx_2 \end{aligned} \quad (28)$$

where $G_{q(\bar{q})/p}(x)$ is the bare PDF.

C. Massless (anti)quark emission

In addition to real gluon emission a second set of real emission corrections to the inclusive cross section for $pp\to\gamma G_{KK}$ at NLO involves the processes with an additional massless $q(\bar{q})$ in the final state:

$$q(\bar{q})g\to\gamma G_{KK}+q(\bar{q}). \quad (29)$$

The relevant Feynman diagrams are shown in Fig. 5. The diagrams for $\bar{q}$ emission are similar and are omitted here.

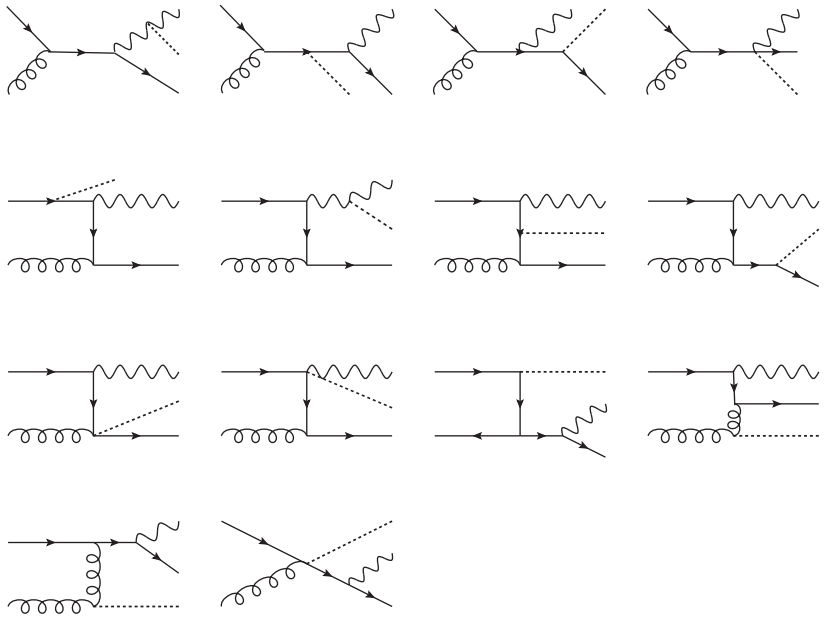

FIG. 5: Feynman diagrams for $qg \to \gamma G_{KK} + q$.

Since the contributions from real massless $q(\bar{q})$ emission contain initial state collinear singularities we need to use the two cutoff phase space slicing method [29] to isolate these collinear divergences. But we only split the phase space into two regions because there are no soft divergences. Consequently, using the approach in Ref. [29], the cross sections for the processes with an additional massless $q(\bar{q})$ in the final state can be expressed as

$$\begin{aligned} d\sigma_m^{add} &= \sum_{(\alpha=g,\beta=q,\bar{q})} \hat{\sigma}_m^{\overline{C}}(\alpha\beta \to \gamma G_{KK} + q(\bar{q}))[G_{\alpha/p}(x_1)G_{\beta/p}(x_2) + (x_1 \leftrightarrow x_2)]dx_1dx_2 \\ &+ d\hat{\sigma}_m^B \left[\frac{\alpha_s}{2\pi}\frac{\Gamma(1-\epsilon)}{\Gamma(1-2\epsilon)}\left(\frac{4\pi\mu_r^2}{s}\right)^{\epsilon}\right](-\frac{1}{\epsilon})\delta_c^{-\epsilon}\left[P_{qg}(z,\epsilon)G_{g/p}(x_1/z)G_{\bar{q}/p}(x_2)\right. \\ &\left. + P_{\bar{q}g}(z,\epsilon)G_{q/p}(x_1)G_{g/p}(x_2/z) + (x_1 \leftrightarrow x_2)\right]\frac{dz}{z}\left(\frac{1-z}{z}\right)^{-\epsilon}dx_1dx_2 \end{aligned} \tag{30}$$

where

$$\begin{aligned} P_{qg}(z) &= P_{\bar{q}g}(z) = \frac{1}{2}[z^2 + (1-z)^2], \\ P'_{qg}(z) &= P'_{\bar{q}g}(z) = -z(1-z). \end{aligned} \tag{31}$$

The $\hat{\sigma}_m^{\overline{C}}$ term in Eq. (30) represents the noncollinear cross sections for the $q(\bar{q})g$ initiated processes which can be written in the form

$$d\hat{\sigma}_m^{\overline{C}} = \frac{1}{2s}\overline{\sum}|M(q(\bar{q})g \overset{\text{noncollinear}}{\longrightarrow} \gamma G_{KK} + q(\bar{q}))|^2 d\bar{\Gamma}_3, \tag{32}$$

where $d\bar{\Gamma}_3$ is the three-body phase space in the noncollinear region. The other terms in Eq. (30) are the collinear singular cross sections.

D. Mass factorization

After adding the renormalized virtual corrections and the real corrections, the parton level cross sections still contain collinear divergences which can be absorbed into a redefinition of the PDFs at NLO, generally called mass factorization[38, 39]. This procedure, in practice, means that first we convolute the partonic cross section with the bare PDF $G_{\alpha/p}(x)$ and then use the renormalized PDF $G_{\alpha/p}(x,\mu_f)$ to replace $G_{\alpha/p}(x)$. In the $\overline{\rm MS}$ convention the scale-dependent PDF $G_{\alpha/p}(x,\mu_f)$ is given by [29]

$$G_{\alpha/p}(x,\mu_f) = G_{\alpha/p}(x) + \sum_\beta \left(-\frac{1}{\epsilon}\right)\left[\frac{\alpha_s}{2\pi}\frac{\Gamma(1-\epsilon)}{\Gamma(1-2\epsilon)}\times\left(\frac{4\pi\mu_r^2}{\mu_f^2}\right)^\epsilon\right] \times\int_x^1 \frac{dz}{z}P_{\alpha\beta}(z)G_{\beta/p}(x/z). \tag{33}$$

This replacement will produce a collinear singular counterterm which is then combined with the hard collinear contributions to give Ref. [29] the $\mathcal{O}(\alpha_s)$ expression for the remaining collinear contribution:

$$\begin{aligned} d\sigma_m^{coll} = d\hat{\sigma}_m^B &\left[\frac{\alpha_s}{2\pi}\frac{\Gamma(1-\epsilon)}{\Gamma(1-2\epsilon)}\left(\frac{4\pi\mu_r^2}{s}\right)^\epsilon\right]\{\tilde{G}_{q/p}(x_1,\mu_f)G_{\bar{q}/p}(x_2,\mu_f)+G_{q/p}(x_1,\mu_f)\tilde{G}_{\bar{q}/p}(x_2,\mu_f)\\ &+\sum_{\alpha=q,\bar{q}}\left[\frac{A_1^{sc}(\alpha\to\alpha g)}{\epsilon}+A_0^{sc}(\alpha\to\alpha g)\right]G_{q/p}(x_1,\mu_f)G_{\bar{q}/p}(x_2,\mu_f)\\ &+(x_1\leftrightarrow x_2)\}dx_1dx_2, \end{aligned} \tag{34}$$

where

$$A_1^{sc}(q\to qg) = A_1^{sc}(\bar{q}\to\bar{q}g) = C_F(2\ln\delta_s+3/2), \tag{35}$$

$$A_0^{sc} = A_1^{sc}\ln(\frac{s}{\mu_f^2}), \tag{36}$$

$$\tilde{G}_{\alpha(=q,\bar{q})/p}(x,\mu_f) = \sum_{\beta=g,\alpha}\int_x^{1-\delta_s\delta_{\alpha\beta}}\frac{dy}{y}G_{\beta/p}(x/y,\mu_f)\tilde{P}_{\alpha\beta}(y) \tag{37}$$

with

$$\tilde{P}_{\alpha\beta}(y) = P_{\alpha\beta}(y)\ln(\delta_c\frac{1-y}{y}\frac{s}{\mu_f^2}) - P'_{\alpha\beta}(y). \tag{38}$$

Finally, the NLO total cross section for $pp \to \gamma G_{KK}$ in the $\overline{\rm MS}$ factorization scheme is

$$\sigma^{NLO} = \int dm\ S_{\delta-1} \frac{\bar{M}_P^2}{M_D^{2+\delta}} m^{\delta-1} \sigma_m^{NLO} \tag{39}$$

with

$$\sigma_m^{NLO} = \int dx_1 dx_2 \{ \Big[G_{q/p}(x_1,\mu_f) G_{\bar{q}/p}(x_2,\mu_f) + (x_1 \leftrightarrow x_2) \Big] (\hat{\sigma}_m^B + \hat{\sigma}_m^V + \hat{\sigma}_m^S + \hat{\sigma}_m^{\overline{HC}}) \} + \sigma_m^{coll}$$
$$+ \sum_{(\alpha=g,\beta=q,\bar{q})} \int dx_1 dx_2 \Big[G_{\alpha/p}(x_1,\mu_f) G_{\beta/p}(x_2,\mu_f) + (x_1 \leftrightarrow x_2) \Big] \hat{\sigma}_m^{\overline{C}}(\alpha\beta \to \gamma G_{KK} + \beta) \tag{40}$$

Note that the above expression contains no singularities since $2A_2^V + A_2^s = 0$ and $2A_1^V + A_1^s + A_1^{sc}(q \to qg) + A_1^{sc}(\bar{q} \to \bar{q}g) = 0$.

IV. NUMERICAL RESULTS

In this section we present numerical results for the total and the differential cross sections for γG_{KK} associated production at the LHC. In our numerical calculations the running QCD coupling constant $\alpha_s(\mu)$ is evaluated at three-loop order[40] and the CTEQ6.6M PDFs[41] are used throughout. Only u and d flavor are activated since numerical calculations show that contributions from other flavor can be omitted. We take the LED parameters M_D and δ as input. Except for the scale uncertainty plot, both the renormalization and the factorization scale are fixed at p_T^γ, which is the transverse momentum of the photon. Jet are defined by the following requirements:

$$\begin{aligned} p_T^{jet} &> 20\text{GeV}, \\ |\eta^{jet}| &< 2.5. \end{aligned} \tag{41}$$

Besides, the following cuts are assumed in our calculations[12, 42]:

$$\begin{aligned} & p_T^\gamma > p_T^{min}, \\ & |\eta| < 2.4, \\ & p_T^{miss} > p_T^{min}, \\ & \Delta\phi(\gamma, p_T^{miss}) > 2.5. \end{aligned} \tag{42}$$

Here the default value of p_T^{min} is 400GeV in the following calculations, as suggested in Ref.[12, 42], η is the pseudorapidity of the photon and p_T^{miss} is the missing transverse momentum,

defined as

$$p_T^{miss} \equiv \begin{cases} p_T^{\gamma}, & \text{no jet in the final state,} \\ p_T^{G}, & \text{with jet in the final state,} \end{cases}$$

where p_T^G is the transverse momentum of the graviton. We also require the photon to be isolated by requiring the separation of the photon and the radiated parton $\Delta R \equiv \sqrt{\Delta\phi^2 + \Delta\eta^2}$ to be greater than 0.4.

Moreover, it should be noted that the LED model is an effective low energy theory. Therefore we present two classes of numerical results to quantify the ultraviolet sensitivity: one with the truncation $m^2_{\gamma G_{KK}} < M_D^2$, $m_{\gamma G_{KK}}$ being the invariant mass of the graviton and the photon, while the other one is not truncated. As pointed out in Ref.[12] if the two results significantly differ the contributions arising from regions above M_D dominate, and the calculations are not under control but if they do not the LED model is viable.

In Fig.6 we show that it is reasonable to use the two cutoff phase space slicing method in our NLO QCD calculations; i.e., the dependence of the NLO QCD predictions on the arbitrary cutoffs δ_s and δ_c is indeed very weak, as was also found in Ref.[29]. While the Born cross sections and the virtual corrections are cutoff independent, both the soft and collinear contributions and the noncollinear contributions depend strongly on the cutoffs. However, the cutoff dependence in the two contributions ($\sigma_m^S + \sigma_m^{coll}$ and $\sigma_m^{\overline{HC}} + \sigma_m^{\overline{C}}$) nearly cancel each other , especially for the cutoff δ_s between 10^{-4} and 10^{-3}, where the final results for σ^{NLO} are almost entirely independent of the cutoffs. Therefore, we will take $\delta_s = 10^{-4}$ in the numerical calculations below. Generally δ_c being $50 - 100$ times smaller than δ_s is sufficient for accurate calculations to a few percent[29], so we take $\delta_c = \delta_s/50$ in our calculations.

Figure 7 shows the dependence of both the LO and the NLO total cross sections on the factorization scale(μ_f) and the renormalization scale(μ_r) assuming $M_D = 2$TeV, $\delta = 4$, and setting $p_T^{min} = 400$GeV. When the scale μ varies from $0.2p_T^{\gamma}$ to $5p_T^{\gamma}$, the LO total cross sections vary from 1.18 to 0.86fb, while the NLO total cross sections vary from 1.13 to 0.91fb. Thus, the NLO corrections reduce the scale dependence, which makes the theoretical predictions somewhat more reliable. The conclusion is similar for $\delta = 2$, which is not shown here.

In Fig.8 and Fig.9 we show the dependence of both the LO and the NLO total cross sections on M_D, setting $p_T^{min} = 400$GeV, and assuming $\delta = 2$ and 4, respectively. As M_D

increases the LO total cross sections decrease and the two results, with and without the truncation, approach each other. Also shown in Fig.8 and Fig.9 are the K factors, defined as σ^{NLO}/σ^{LO}, which are around $1.3 \sim 1.5$ for $\delta = 2$ and $1.1 \sim 1.3$ for $\delta = 4$, respectively. We also give K factors for cases with jet veto[42], where events with $p_T^{jet} > 100$GeV are vetoed. In this case, the K factors are around $0.9 \sim 1$ for $\delta = 2$ and $0.8 \sim 0.9$ for $\delta = 4$, respectively, i.e., the NLO corrections reduce the LO results, which is due to the fact that the jet veto discards large positive contributions from real emission processes.

In Fig.10 and Fig.11 we show the dependence of both the LO and the NLO total cross sections on p_T^{min}, for $M_D = 3$TeV and $\delta = 2$ and 4, respectively. As p_T^{min} increases the LO total cross sections decrease and the two results, with and without the truncation, differ increasingly. The K factors are about $1.3 \sim 1.4$ for $\delta = 2$ and 1.2 for $\delta = 4$, respectively. When jet veto is considered, the K factors are around 0.95 for $\delta = 2$ and $0.84 \sim 0.9$ for $\delta = 4$, respectively.

In Figs.12-14 we display differential cross sections with truncation as functions of the missing transverse momentum, the transverse momentum and the pseudorapidity of photon, respectively. We find that the NLO QCD corrections always enhance the LO differential cross sections but do not significantly change the shapes of the LO differential cross sections.

In conclusion, we have calculated the complete NLO QCD corrections to the inclusive total cross sections for γG_{KK} associated production in the LED model at the LHC. The NLO corrections generally enhance the total cross sections and the K factor is around $1.3 \sim 1.5$ for $\delta = 2$ and $1.1 \sim 1.3$ for $\delta = 4$, respectively. When jet veto is considered, the NLO contributions reduce the LO results, the K factors are around $0.9 \sim 1$ for $\delta = 2$ and $0.8 \sim 0.9$ for $\delta = 4$, respectively. We also compared the results with and without truncation of $m_{\gamma G_{KK}}$ to quantify the ultraviolet sensitivity of the LED model. The NLO QCD corrections were found to reduce the dependence of the total cross sections on the renormalization/factorization scale. We also calculated some important differential distributions for this process at the NLO, including the missing transverse momentum distribution, the transverse momentum distribution and the pseudorapidity distribution of photon. We found that the NLO corrections enhance these LO differential cross sections but do not appreciably change their shapes.

Acknowledgements

This work is supported in part by the National Natural Science Foundation of China under grants No.10721063, No.10975004, and No.10635030, and the US Department of Energy, Division of High Energy Physics under Grant No. DE-FG02-91-ER4086.

APPENDIX A

In this appendix we give the related Feynman rules[11][12].

$\bar{q}(k_2)q(k_1)G_{\mu\nu}$: $\quad -i\frac{\kappa}{8}[\gamma_\mu(k_1-k_2)_\nu+\gamma_\nu(k_1-k_2)_\mu]$,

$V_\alpha(k_1)V_\beta(k_2)G_{\mu\nu}$: $\quad -i\frac{\kappa}{2}[k_1\cdot k_2 C_{\mu\nu,\alpha\beta}+D_{\mu\nu,\alpha\beta}(k_1,k_2)+E_{\mu\nu,\alpha\beta}(k_1,k_2)]$,

$\bar{q}(k_2)q(k_1)V^a_\alpha G_{\mu\nu}$: $\quad i\frac{\kappa}{4}gT^a(C_{\mu\nu,\alpha\beta}-\eta_{\mu\nu}\eta_{\alpha\beta})\gamma^\beta$.

In all the Feynman rules the particle momenta flow inward, gT^a represents either g_sT^a if V is a gluon or eQ_f if V is a photon and

$$\begin{aligned}
C_{\mu\nu,\alpha\beta} &= \eta_{\mu\alpha}\eta_{\nu\beta}+\eta_{\mu\beta}\eta_{\nu\alpha}-\eta_{\mu\nu}\eta_{\alpha\beta},\\
D_{\mu\nu,\alpha\beta}(k_1,k_2) &= \eta_{\mu\nu}k_{1\beta}k_{2\alpha}-[\eta_{\mu\beta}k_{1\nu}k_{2\alpha}+\eta_{\mu\alpha}k_{1\beta}k_{2\nu}-\eta_{\alpha\beta}k_{1\mu}k_{2\nu}+(\mu\leftrightarrow\nu)],\\
E_{\mu\nu,\alpha\beta}(k_1,k_2) &= \eta_{\mu\nu}(k_{1\alpha}k_{1\beta}+k_{2\alpha}k_{2\beta}+k_{1\alpha}k_{2\beta})-[\eta_{\nu\beta}k_{1\mu}k_{1\alpha}+\eta_{\nu\alpha}k_{2\mu}k_{2\beta}+(\mu\leftrightarrow\nu)] \quad (43)
\end{aligned}$$

APPENDIX B

We collect the explicit expressions of the finite terms of the matrix element squared in this appendix. $\mathcal{S}$ in Eq.(12) is given by

$$\begin{aligned}
\mathcal{S} =&\frac{\kappa^2Q_q^2}{6}\{\frac{1}{ut}[3C_0^2t(m^2-4t)(m^4-2tm^2+s^2+t^2)-3C_0^5(m^2-4t)(m^2-t)(m^4-2tm^2+s^2\\
&+t^2)-3D_0^1st(m^2-4t)(m^4-2tm^2+s^2+t^2)+3D_0^2su(2s^2+2ts+t^2)(3m^2-4(s+t))\\
&+3C_0^6(2s^3+4ts^2+3t^2s+t^3)(3m^2-4(s+t))+3C_0^3u(2s^2+2ts+t^2)(4(s+t)-3m^2)
\end{aligned}$$

$$
\begin{aligned}
&- 3C_0^4(m^2-s)(m^6-6tm^4+(-5s^2-6ts+6t^2)m^2+4s(2s^2+3ts+3t^2))\\
&- 3C_0^1((s+8t)m^6-6t(s+4t)m^4+(7s^3+18ts^2+30t^2s+32t^3)m^2-4(2s^4+5ts^3\\
&+ 9t^2s^2+8t^3s+4t^4))]+\frac{1}{stu}[2((3s+14t)m^6-6(s^2+5ts+t^2)m^4+(3s^3+30ts^2\\
&- 16t^3)m^2+2t(-7s^3-3ts^2+8t^2s+4t^3))+18(-(s+5t)m^6+(s^2+8ts+11t^2)m^4\\
&- (s^3+8ts^2+15t^2s+12t^3)m^2+t(5s^3+11ts^2+12t^2s+6t^3))]+\\
&\frac{1}{stu(m^2-s)^2(m^2-t)^2(s+t)^2}[3s((3s^2+4ts-2t^2)m^{12}-2(3s^3+16ts^2+17t^2s\\
&+ 4t^3)m^{10}+(6s^4+22ts^3+56t^2s^2+68t^3s+34t^4)m^8-2(3s^5-5ts^4-41t^2s^3\\
&- 46t^3s^2+5t^4s+18t^5)m^6+(3s^6+2ts^5-110t^2s^4-300t^3s^3-266t^4s^2-60t^5s\\
&+ 12t^6)m^4+2st(-3s^5+14ts^4+86t^2s^3+137t^3s^2+84t^4s+16t^5)m^2\\
&- 24s^2t^3(s+t)^3)\log\left(\frac{m^2}{\mu^2}\right)m^2-3s(m^2-t)^2(s+t)^2(3m^{10}-6(s+3t)m^8+6(s^2+3ts\\
&+ 3t^2)m^6-2s^2(3s+11t)m^4+s^2(3s^2+42ts+22t^2)m^2-20s^3t(s+t))\log\left(\frac{s}{\mu^2}\right)\\
&- (m^2-s)((m^2-t)((s+t)^2(21s+34t)m^{10}-(18s^4+196ts^3+483t^2s^2+441t^3s\\
&+ 136t^4)m^8+(s+t)^2(15s^3+165ts^2+466t^2s+238t^3)m^6-(18s^6+124ts^5+587t^2s^4\\
&+ 1473t^3s^3+1786t^4s^2+998t^5s+204t^6)m^4+t(s+t)^2(49s^4+154ts^3+382t^2s^2\\
&+ 340t^3s+68t^4)m^2-2st^2(s+t)^3(11s^2+34ts+34t^2)-3(m^2-s)s(m^2-t)t((2s\\
&+ 5t)m^6-6t(s+t)m^4+3(2s-t)(s+t)^2m^2-4(2s-t)(s+t)^3)\log\left(-\frac{u}{\mu^2}\right))\\
&- 3st(s+t)^2(3(4s+3t)m^8-(24s^2+57ts+22t^2)m^6+(12s^3+75ts^2+74t^2s\\
&+ 17t^3)m^4-t(27s^3+64ts^2+33t^2s+4t^3)m^2+4st^2(3s^2+4ts+t^2))\log\left(-\frac{t}{\mu^2}\right))]\},
\end{aligned}
\tag{44}
$$

where Q_q is the electric charge of the initial (anti)quark, and

$$
\begin{aligned}
C_0^1 &= -\frac{\pi^2}{3s}, \\
C_0^2 &= \frac{1}{2t}(\log^2\left(\frac{-t}{s}\right) + \frac{\pi^2}{3}), \\
C_0^3 &= \frac{1}{2u}(\log^2\left(\frac{-u}{s}\right) + \frac{\pi^2}{3}), \\
C_0^4 &= \frac{\log^2\left(\frac{m^2}{s}\right)}{2(m^2-s)}, \\
C_0^5 &= \frac{1}{2(m^2-t)}[\log\left(\frac{m^2}{-t}\right)(\log\left(\frac{m^2}{s}\right) + \log\left(\frac{-t}{s}\right)) - \pi^2], \\
C_0^6 &= \frac{1}{2(m^2-u)}[\log\left(\frac{m^2}{-u}\right)(\log\left(\frac{m^2}{s}\right) + \log\left(\frac{-u}{s}\right)) - \pi^2], \\
D_0^1 &= \frac{1}{st}[-\log^2\left(\frac{m^2}{s}\right) + \pi^2 - 2\mathrm{Li}_2(1-\frac{m^2}{s}) - 2\mathrm{Li}_2(1-\frac{m^2}{t})], \\
D_0^2 &= \frac{1}{su}[-\log^2\left(\frac{m^2}{s}\right) + \pi^2 - 2\mathrm{Li}_2(1-\frac{m^2}{s}) - 2\mathrm{Li}_2(1-\frac{m^2}{u})]. \qquad (45)
\end{aligned}
$$

---

[1] N. Arkani-Hamed, S. Dimopoulos, and G. R. Dvali, Phys. Lett. **B429**, 263 (1998).

[2] N. Arkani-Hamed, S. Dimopoulos, and G. R. Dvali, Phys. Rev. **D59**, 086004 (1999).

[3] I. Antoniadis, N. Arkani-Hamed, S. Dimopoulos, and G. R. Dvali, Phys. Lett. **B436**, 257 (1998).

[4] L. Randall and R. Sundrum, Phys. Rev. Lett. **83**, 3370 (1999).

[5] L. Randall and R. Sundrum, Phys. Rev. Lett. **83**, 4690 (1999).

[6] J. D. Lykken, Phys. Rev. **D54**, 3693 (1996).

[7] E. Witten, Nucl. Phys. **B471**, 135 (1996).

[8] P. Horava and E. Witten, Nucl. Phys. **B460**, 506 (1996).

[9] P. Horava and E. Witten, Nucl. Phys. **B475**, 94 (1996).

[10] I. Antoniadis, Phys. Lett. **B246**, 377 (1990).

[11] T. Han, J. D. Lykken, and R.-J. Zhang, Phys. Rev. **D59**, 105006 (1999).

[12] G. F. Giudice, R. Rattazzi, and J. D. Wells, Nucl. Phys. **B544**, 3 (1999).

[13] E. G. Adelberger (EOT-WASH Group) (2002), hep-ex/0202008.

[14] K. Cheung (2004), hep-ph/0409028.

[15] P. Mathews, V. Ravindran, K. Sridhar, and W. L. van Neerven, Nucl. Phys. **B713**, 333 (2005).

[16] P. Mathews, V. Ravindran, and K. Sridhar, JHEP **10**, 031 (2005).

[17] P. Mathews and V. Ravindran, Nucl. Phys. **B753**, 1 (2006).

[18] M. C. Kumar, P. Mathews, and V. Ravindran, Eur. Phys. J. **C49**, 599 (2007).

[19] Q. Li, C. S. Li, and L. L. Yang, Phys. Rev. **D74**, 056002 (2006).

[20] M. C. Kumar, P. Mathews, V. Ravindran, and A. Tripathi, Phys. Lett. **B672**, 45 (2009).

[21] M. C. Kumar, P. Mathews, V. Ravindran, and A. Tripathi, Nucl. Phys. **B818**, 28 (2009).

[22] N. Agarwal, V. Ravindran, V. K. Tiwari, and A. Tripathi (2009), 0910.1551.

[23] S. Karg, M. Kramer, Q. Li, and D. Zeppenfeld (2009), 0911.5095.

[24] G. 't Hooft and M. J. G. Veltman, Nucl. Phys. **B44**, 189 (1972).

[25] A. Sirlin, Phys. Rev. **D22**, 971 (1980).

[26] W. J. Marciano and A. Sirlin, Phys. Rev. **D22**, 2695, Erratum (1980).

[27] A. Sirlin and W. J. Marciano, Nucl. Phys. **B189**, 442 (1981).

[28] K. I. Aoki, Z. Hioki, M. Konuma, R. Kawabe, and T. Muta, Prog. Theor. Phys. Suppl. **73**, 1 (1982).

[29] B. W. Harris and J. F. Owens, Phys. Rev. **D65**, 094032 (2002).

[30] G. P. Lepage, J. Comput. Phys. **27**, 192 (1978).

[31] J. C. Collins, D. E. Soper, and G. Sterman, Nucl. Phys. **B261**, 104 (1985).

[32] G. T. Bodwin, Phys. Rev. **D31**, 2616 (1985).

[33] G. Altarelli and G. Parisi, Nucl. Phys. **B126**, 298 (1977).

[34] R. K. Ellis, D. A. Ross, and A. E. Terrano, Nucl. Phys. **B178**, 421 (1981).

[35] L. J. Bergmann (1989), uMI-89-15738.

[36] Z. Kunszt and D. E. Soper, Phys. Rev. **D46**, 192 (1992).

[37] M. L. Mangano, P. Nason, and G. Ridolfi, Nucl. Phys. **B373**, 295 (1992).

[38] G. Altarelli, R. K. Ellis, and G. Martinelli, Nucl. Phys. **B157**, 461 (1979).

[39] J. C. Collins, D. E. Soper, and G. Sterman, Adv. Ser. Direct. High Energy Phys. **5**, 1 (1988).

[40] C. Amsler et al. (Particle Data Group), Phys. Lett. **B667**, 1 (2008).

[41] P. M. Nadolsky et al., Phys. Rev. **D78**, 013004 (2008), 0802.0007.

[42] G. L. Bayatian et al. (CMS), J. Phys. **G34**, 995 (2007).

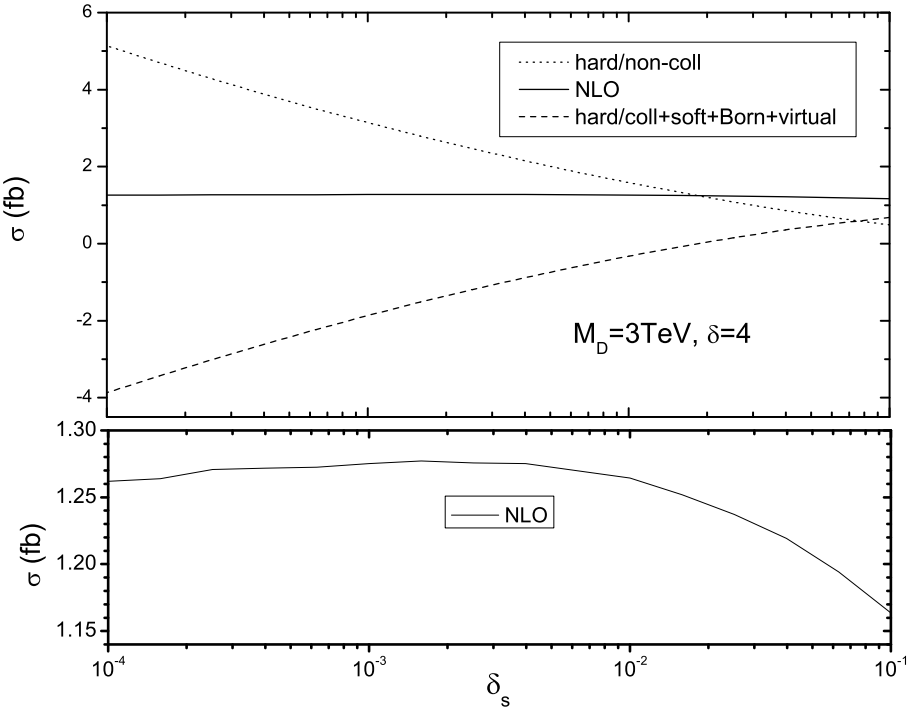

FIG. 6: Dependence of the NLO total cross sections for the γG_{KK} associated production at the LHC on the theoretical cutoff δ_s with $\delta_c = \delta_s/50$, assuming $M_D = 3\text{TeV}$, $\delta = 4$. Truncation $m^2_{\gamma G_{KK}} < M_D^2$ is used here.

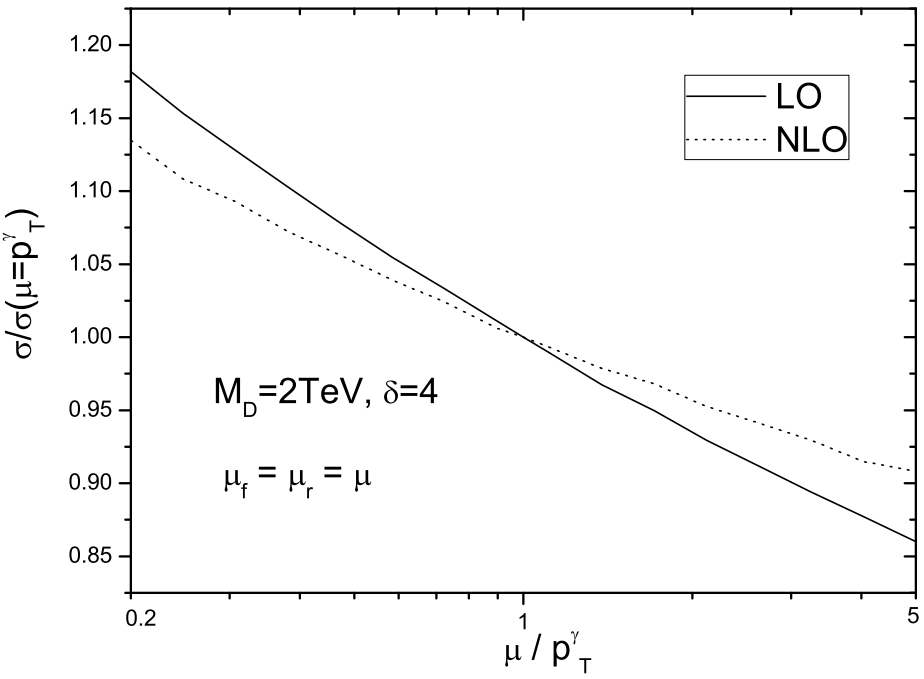

FIG. 7: Dependence of the NLO total cross sections for the γG_{KK} associated production at the LHC on the factorization scale(μ_f) and the renormalization scale(μ_r), assuming $M_D = 2$TeV, $\delta = 4$. Truncation $m^2_{\gamma G_{KK}} < M_D^2$ is used here.

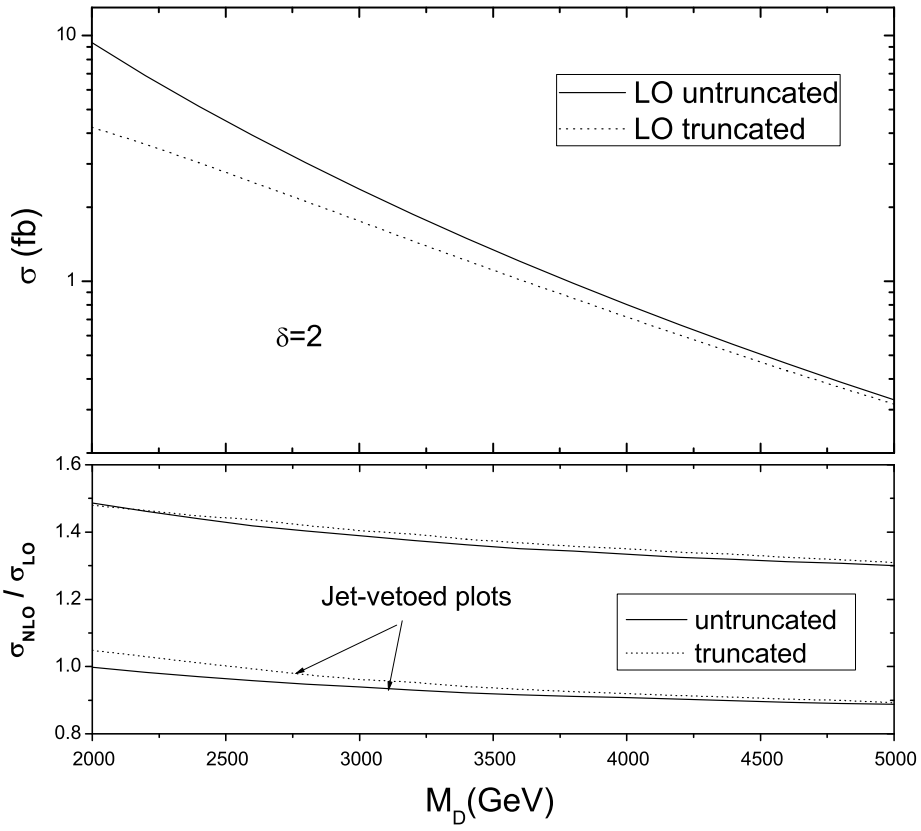

FIG. 8: Dependence of the total cross section of the γG_{KK} associated production at the LHC on M_D, assuming $\delta = 2$.

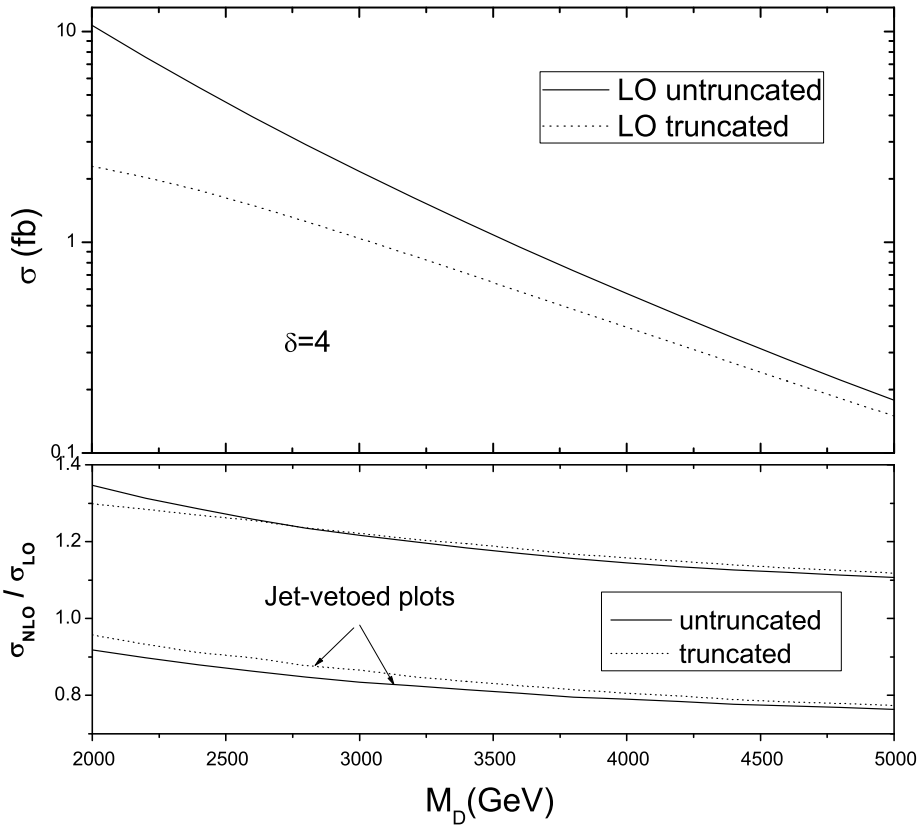

FIG. 9: Dependence of the total cross section of the γG_{KK} associated production at the LHC on M_D, assuming $\delta = 4$.

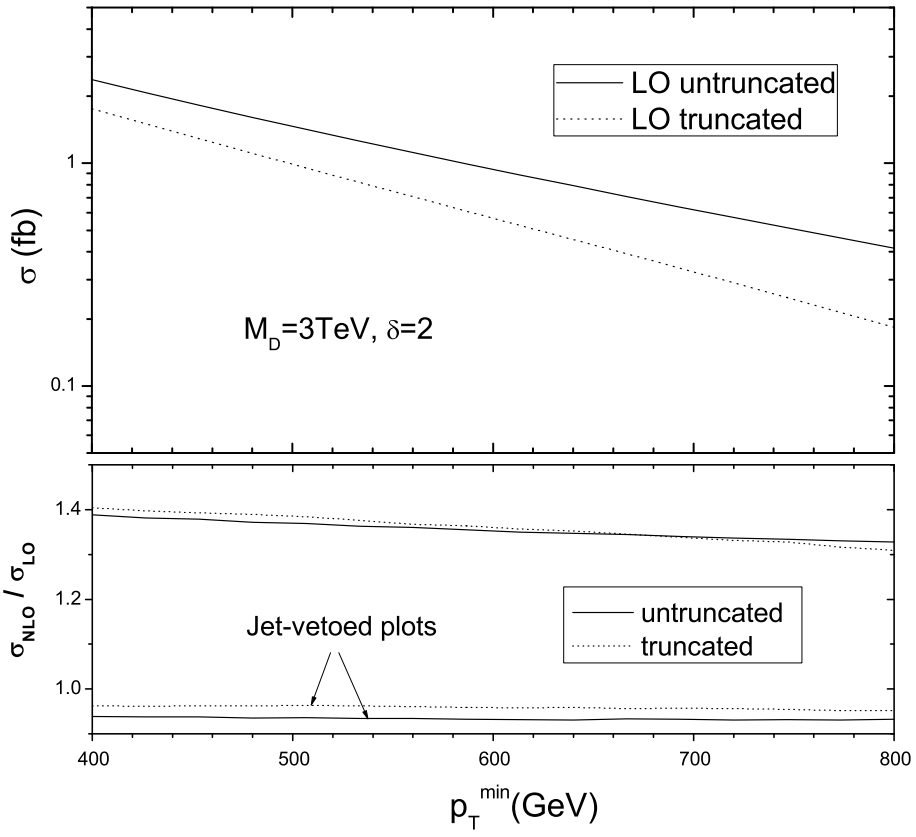

FIG. 10: Dependence of the total cross section of the γG_{KK} associated production at the LHC on p_T^{min}, assuming $M_D = 3\text{TeV}$, $\delta = 2$.

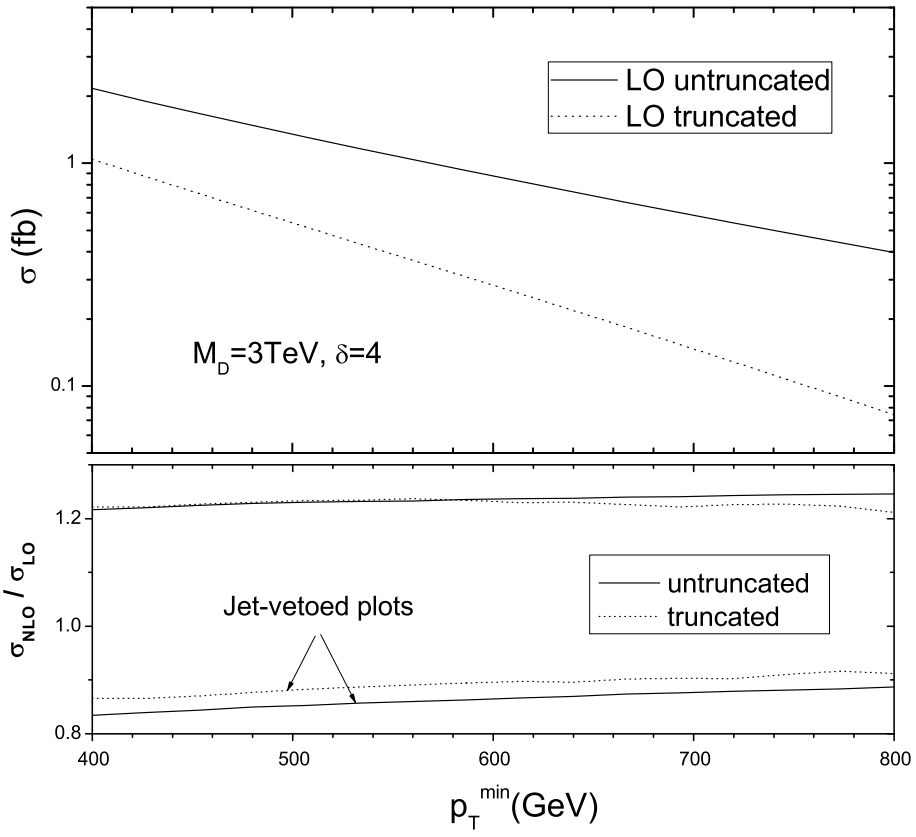

FIG. 11: Dependence of the total cross section of the γG_{KK} associated production at the LHC on p_T^{min}, assuming $M_D = 3\text{TeV}$, $\delta = 4$.

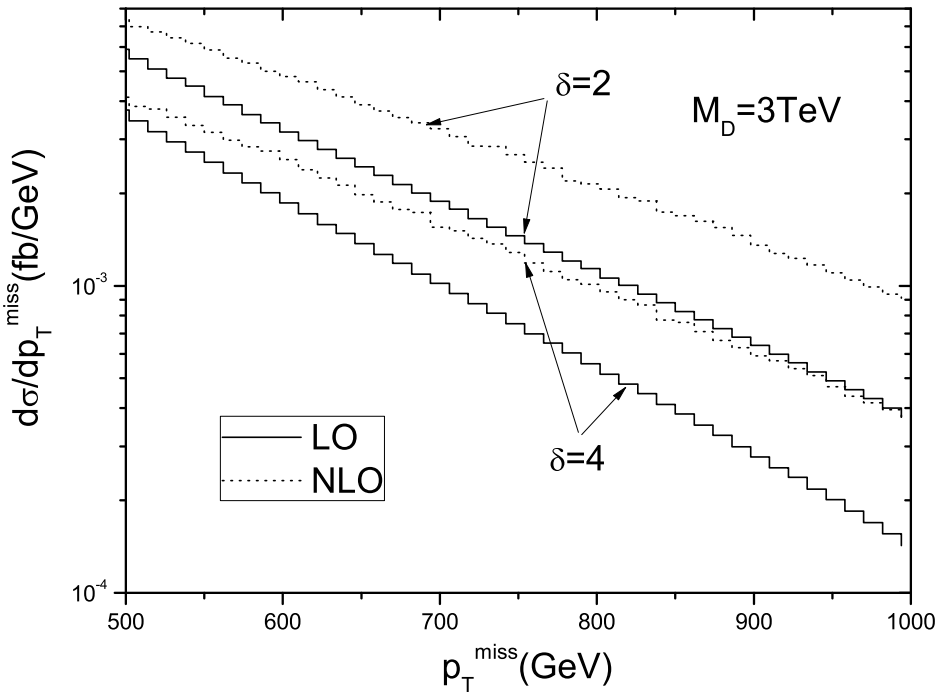

FIG. 12: Dependence of the differential cross section of the γG_{KK} associated production at the LHC on p_T^{miss}, assuming $M_D = 3$TeV, $\delta = 2$ and 4, respectively.

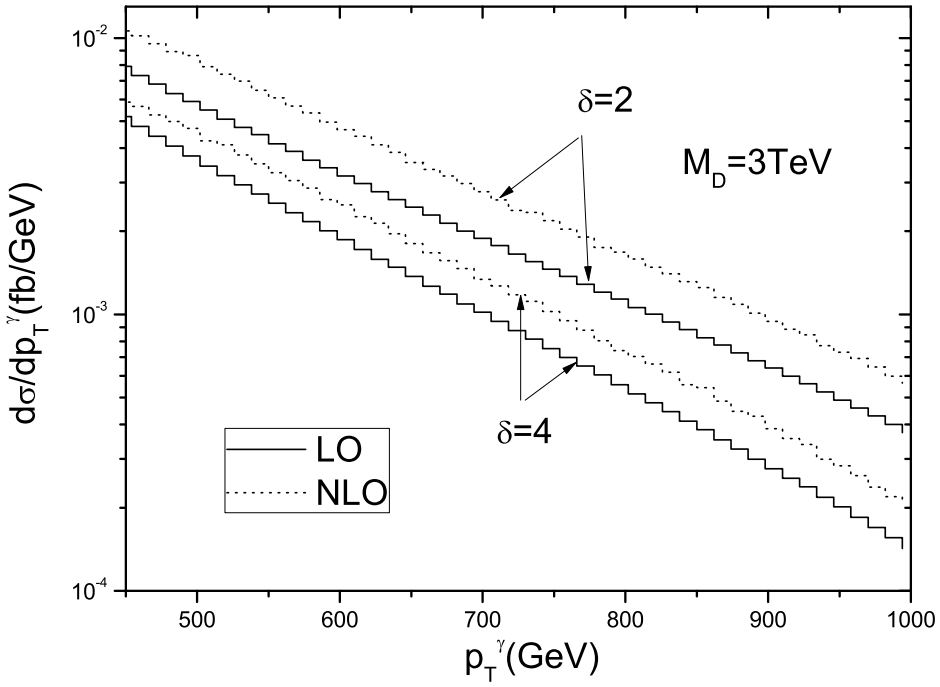

FIG. 13: Dependence of the differential cross section of the γG_{KK} associated production at the LHC on p_T^{γ}, assuming $M_D = 3$TeV, $\delta = 2$ and 4, respectively.

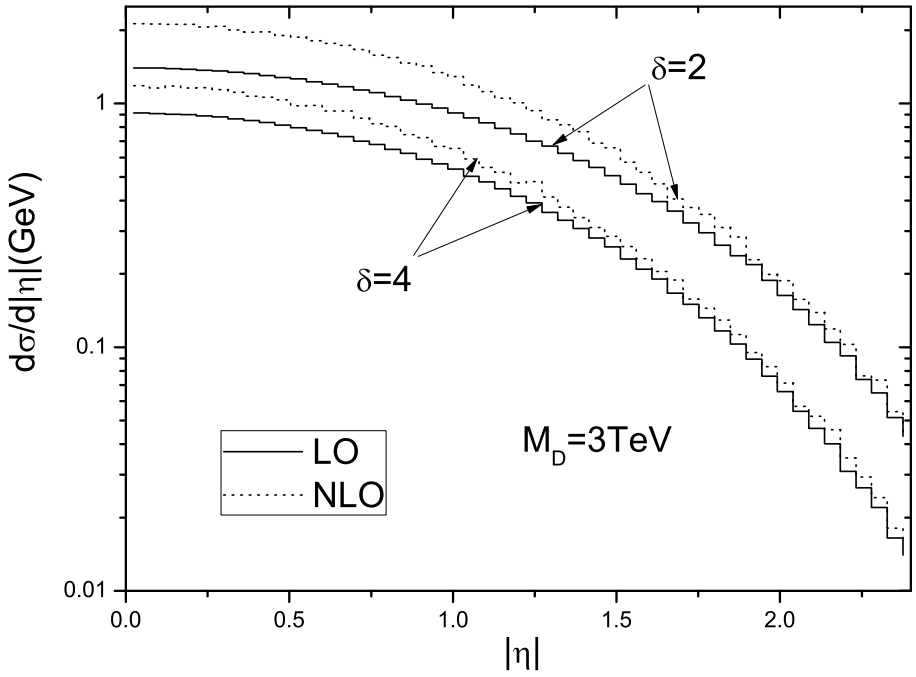

FIG. 14: Dependence of the differential cross section of the γG_{KK} associated production at the LHC on $|\eta|$, assuming $M_D = 3\text{TeV}$, $\delta = 2$ and 4, respectively.